

Magnetic structure of antiferromagnetic NdRhIn₅S. Chang,^{1,2,*} P. G. Pagliuso,^{1,3} W. Bao,¹ J. S. Gardner,⁴ I. P. Swainson,⁴ J. L. Sarrao,¹ and H. Nakotte²¹*Los Alamos National Laboratory, Los Alamos, New Mexico 87545*²*Physics Department, New Mexico State University, Las Cruces, New Mexico 88003*³*DEQ-IFGW-UNICAMP, Cidade Universitaria-Barao, Geraldo 13083-970 Campinas-SP, Brazil*⁴*NRC Canada, NPMR, Chalk River Laboratories, Chalk River, Ontario, Canada K0J 1J0*

(Received 10 May 2002; published 30 October 2002)

The magnetic structure of antiferromagnetic NdRhIn₅ has been determined using neutron diffraction. It has a commensurate antiferromagnetic structure with a magnetic wave vector ($\frac{1}{2}0\frac{1}{2}$) below $T_N=11$ K. The staggered Nd moment at 1.6 K is $2.5(1)\mu_B$ aligned along the c axis. This magnetic structure is closely related to the low-temperature magnetic structure of the cubic parent compound NdIn₃.

DOI: 10.1103/PhysRevB.66.132417

PACS number(s): 75.25.+z, 75.30.Gw, 75.40.Cx

NdRhIn₅ crystallizes in the tetragonal HoCoGa₅ structure (space group $P4/mmm$),¹ and belongs to a large structural family of compounds with the chemical composition R_mMIn_{3m+2} , with R = rare earth, M = transition metal, and $m=1,2$. The tetragonal crystal structures of these compounds may be seen as m layers of RIn_3 and a layer of MIn_2 alternately stacked along the c axis. Included in this family are three newly discovered heavy-Fermion superconductors that have received considerable attention.²⁻⁴ For example, CeRhIn₅, an antiferromagnet below $T_N=3.8$ K, undergoes a transition to a superconducting state at approximately 16 kbar with $T_c=2.1$ K.^{2,5} Another member, CeCoIn₅ is an ambient pressure superconductor with a record setting $T_c=2.3$ K for heavy-Fermion superconductors.⁴ Thermodynamic and transport measurements are indicative of unconventional superconductivity in which there may be line nodes in the superconducting gap.^{6,7}

It is widely held that magnetic ground states of heavy-Fermion compounds are determined by the balance between competing Kondo and Ruderman-Kittel-Kasuya-Yosida (RKKY) interactions.⁸ For f -electron magnetic materials, anisotropy is also known to affect the magnetic state.⁹ Therefore studies of structurally related non-Kondo magnetic materials such as NdRhIn₅ may give insight into the evolution of magnetic properties in these materials.¹⁰ For the present study, we have performed both powder and single-crystal neutron diffraction in order to determine the magnetic structure of the antiferromagnet NdRhIn₅. The results are compared to those of cubic NdIn₃, which may be considered the parent compound in the Nd _{m} MIn _{$3m+2$} series. Further comparisons are also made with the evolution of magnetic structures in the Ce-based series.

Single crystals of NdRhIn₅ were grown from an In flux. The lattice parameters are $a=4.630$ Å and $c=7.502$ Å at room temperature.¹⁰ Neutron-diffraction experiments were performed at Chalk River Laboratories using the C-2 High Resolution Powder Diffractometer and the C-5 triple axis spectrometer in a two axis mode. Incident neutrons of wavelength 1.33 Å were selected using a Si monochromator for C-2, while 1.53-Å neutrons were selected with a Ge monochromator for C-5. In both cases, the sample temperature was regulated by a top loading pumped He cryostat.

In order to determine the magnetic propagation vector, powder-diffraction patterns were collected above and below the ordering temperature using C-2. The low-temperature pattern clearly shows additional magnetic reflections which can be indexed using a magnetic structure with the propagation vector $\mathbf{q}_M=(\frac{1}{2}0\frac{1}{2})$. This corresponds to a magnetic unit cell that doubles the chemical unit cell along the tetragonal a and c axes and contains four magnetic Nd ions.

Subsequently, a rectangular platelike sample of dimensions $\sim 3 \times 3 \times 0.7$ mm³ with the (001) plane the largest surface was measured on C-5. The sample was mounted with the [010] direction vertical in order to access reciprocal-lattice points of the type ($h0l$).

We observed temperature-dependent magnetic Bragg reflections at $(m/2,0,n/2)$, where m and n are odd integers, confirming the propagation vector found in powder diffraction. A typical elastic rocking scan taken at 1.6 K is shown in Fig. 1(a). The intensity of the $(\frac{3}{2}0\frac{1}{2})$ peak is shown in Fig. 1(b) as the square of the order parameter of the antiferromagnetic transition. The Néel temperature was determined to be 11.0(1) K, in good agreement with T_N found in specific-heat measurements.¹⁰ The integrated intensities of magnetic Bragg reflections from such rocking scans were normalized to the (400) and (004) nuclear peaks to yield magnetic cross sections $\sigma_{obs}(\mathbf{q})=I(\mathbf{q})\sin(2\theta)$ in absolute units. The propagation vector \mathbf{q}_M suggests a model in which Nd moments are aligned antiparallel in the [100] and [001] directions, and parallel in the [010] direction, resulting in the magnetic cross section¹¹

$$\sigma(\mathbf{q})=\left(\frac{\gamma r_0}{2}\right)^2 \langle m \rangle^2 |f(q)|^2 \langle 1 - (\hat{\mathbf{q}} \cdot \hat{\mathbf{m}})^2 \rangle, \quad (1)$$

where $\gamma r_0/2=0.2695 \times 10^{-12}$ cm/ μ_B is the scattering length associated with $1\mu_B$, $\langle m \rangle$ is the staggered moment of the Nd ion, and $f(q)$ is the Nd³⁺ magnetic form factor.¹² The polarization factor $\langle 1 - (\hat{\mathbf{q}} \cdot \hat{\mathbf{m}})^2 \rangle$, averaged over possible magnetic domains with the assumption of equal occupation of the domains, is

$$\langle 1 - (\hat{\mathbf{q}} \cdot \hat{\mathbf{m}})^2 \rangle = 1 - \frac{\sin^2 \alpha \sin^2 \beta + 2 \cos^2 \alpha \cos^2 \beta}{2}, \quad (2)$$

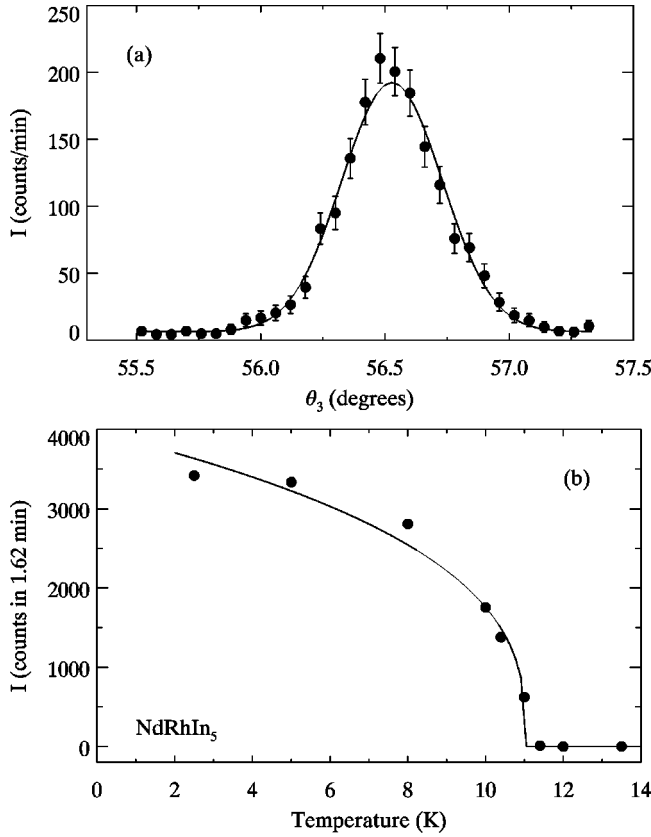


FIG. 1. (a) Elastic rocking scan through magnetic Bragg point $(\frac{1}{2}0\frac{5}{2})$ at 1.6 K. (b) Intensity of $(\frac{3}{2}0\frac{1}{2})$ reflection as a function of temperature. The Néel temperature is 11 K. The solid line is a guide for the eye.

where α is the angle between \mathbf{q} and the c axis, and β is the angle between the magnetic moment and the c axis. The best least-squares fit to Eqs. (1) and (2) gives, within one standard deviation, $\beta=0$, which corresponds to magnetic moments aligned along the c axis, and reduces Eq. (1) to

$$\sigma(\mathbf{q}) = \left(\frac{\gamma r_0}{2}\right)^2 \langle m \rangle^2 |f(q)|^2 (1 - \cos^2 \alpha). \quad (3)$$

The best least squares fit of the experimental data was achieved using the spin-only Nd^{3+} form factor. Such a fit results in a staggered Nd moment at 1.6 K of $\langle m \rangle = 2.61(1)\mu_B$. Figure 2 shows the quantity $\sigma(q)/[(\gamma r_0/2)^2 \langle m \rangle^2 (1 - \cos^2 \alpha)]$, which is equal to the square of the magnetic form factor, $|f|^2$ [refer to Eq. (3)]. The solid line in Fig. 2 is the theoretical spin-only Nd^{3+} form factor.¹²

The high-temperature effective moment of $3.66\mu_B$, deduced from susceptibility data above 150 K, is in good agreement with the Hund's rule value of $3.62\mu_B$, indicating well localized Nd moments at high temperatures.¹⁰ One thus expects some orbital contribution to the magnetic moment. The lower staggered moment of $2.61\mu_B$ found here, at 1.6 K, reflects the presence of crystalline electric field (CEF) effects.⁹ We performed additional least-squares fits of the data using the orbit-only and spin+orbit form factors,¹² represented by the dotted and dashed lines in Fig. 2, respec-

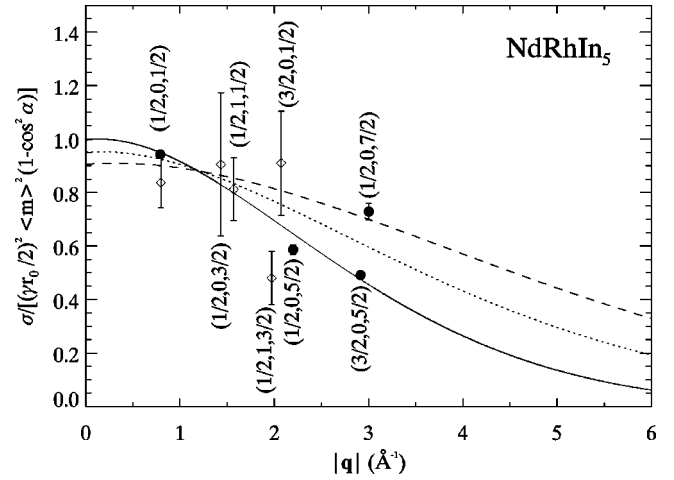


FIG. 2. The q dependence of the square of the magnetic form factor, $|f|^2$ as given by the quantity, $\sigma(q)/[(\gamma r_0/2)^2 \langle m \rangle^2 (1 - \cos^2 \alpha)]$ [refer to Eq. (3)]. Single-crystal data are shown as solid circles, while data from the powder-diffraction experiment are represented by open diamonds. The value of the staggered Nd moment, $\langle m \rangle = 2.61\mu_B$ was taken from the best least-squares fit of the data, which was achieved using the spin-only Nd^{3+} form factor. The solid line is the theoretical spin-only Nd^{3+} form factor. Analysis using the orbit-only form factor resulted in a lower staggered moment of $2.50(1)\mu_B$. Since the data have been normalized to $\langle m \rangle = 2.61\mu_B$, determined with the spin-only form factor, the dotted line, which represents the orbit-only form factor, has a lower intercept on this scale, reflecting a lower staggered moment. Similarly, the spin+orbit form factor (dashed line) also resulted in a smaller moment of $2.39(1)\mu_B$. All Nd^{3+} form factors were taken from Ref. 12.

tively. Note that the data points in Fig. 2 were normalized to $\langle m \rangle = 2.61\mu_B$, determined with the spin-only form factor. On this scale, the best fits of the orbit-only and spin+orbit form factors intersect the vertical axis, at $|\mathbf{q}|=0$, at lower values. Since by definition, $|f(\mathbf{q}=0)|^2=1$, the dotted and dashed lines in Fig. 2 indicate that these fits result in lower Nd moments. For instance, using the spin+orbit form factor gives a staggered moment of $2.39(1)\mu_B$ and using the orbit-only form factor results in a staggered moment of $2.50(1)\mu_B$. Unfortunately, our experiment cannot determine exactly the orbital contribution to the magnetic moment. Therefore we take the results of the fits using the spin-only (solid line) and spin+orbit (dashed line) form factors to be the upper and lower bounds to the staggered moment, respectively. This yields a staggered moment of about $2.5(1)\mu_B$ per Nd.

Now, we compare the magnetic structure of NdRhIn_5 with that of its cubic parent compound NdIn_3 , which orders antiferromagnetically below $T_N=6$ K and exhibits a complex magnetic phase diagram, including two additional antiferromagnetic transitions at 4.61 and 5.13 K.¹³⁻¹⁵ The two intermediate phases were determined to have incommensurate structures with magnetic propagation vectors $\mathbf{q}_M = (\frac{1}{2}0.037\frac{1}{2})$ and $(\frac{1}{2}0.017\frac{1}{2})$, respectively, while the ground-state structure was determined to be commensurate with $\mathbf{q}_M = (\frac{1}{2}0\frac{1}{2})$ and staggered Nd moments of approximately $2.0\mu_B$ with $[010]$ the easy magnetization direction.^{16,17} The

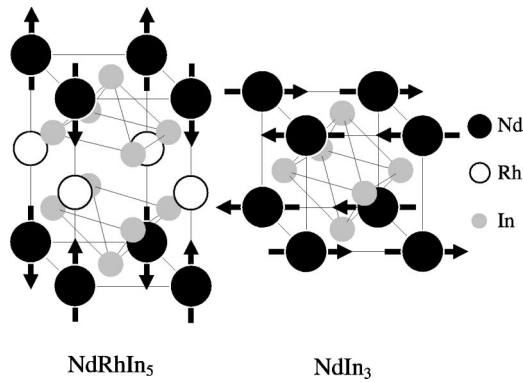


FIG. 3. Schematic representation of the crystallographic and magnetic structure of NdRhIn_5 in a chemical unit cell. The commensurate magnetic structure of NdIn_3 below 4.6 K from Ref. 17 is also shown for comparison. The arrows indicate the directions of the Nd moments.

complexity of the magnetic phase diagram of NdIn_3 was also verified by various field-induced transitions in the H - T phase diagram.^{16,17} A model including competing CEF and magnetic exchange anisotropies has satisfactorily described the complex phase diagrams of NdIn_3 .¹⁷

The magnetic structure of NdRhIn_5 is shown together with that of NdIn_3 below 4.6 K in Fig. 3. In comparison to NdIn_3 , the moment direction relative to the magnetic wave vector is rotated by 90° in NdRhIn_5 . However, the phases among the magnetic moments are identical in both cases.

For the tetragonal NdRhIn_5 , the insertion of a RhIn_2 layer nearly doubles the Néel temperature of NdIn_3 . No evidence of additional transitions below T_N was observed in our study as well as in bulk measurements down to 1 K.¹⁰ In addition, field-dependent heat capacity revealed no evidence for field-induced transitions up to $H=9$ T applied in the ab plane and one transition at about 7 T for $H\parallel c$ axis.¹⁸ Therefore, although the magnetic structure of NdRhIn_5 is closely related to the parent compound NdIn_3 , the relatively simple H - T phase diagram of NdRhIn_5 suggests that the commensurate antiferromagnetic structure $\mathbf{q}_M=(\frac{1}{2}0\frac{1}{2})$ is more robust and stable in the tetragonal variant. In fact, the $\text{Nd}^{3+}(J=9/2)$ ion

in axial symmetry commonly has its multiplet split in anisotropic doublets (with $g_{\parallel c} \gg g_{\perp}$) favoring the Nd spins to point along the c axis which is consistent with our results. Therefore the tetragonal symmetry may produce an improved matching among the existing CEF, magnetocrystalline and exchange coupling anisotropies for NdRhIn_5 .

We now extend our discussion to the Ce-based series. For CeRhIn_5 , the nearest-neighbor antiferromagnetic structure of the parent compound CeIn_3 is maintained within the CeIn_3 layers. However, the magnetic moments in CeRhIn_5 form an incommensurate spiral along the c axis.^{19,20} Furthermore, T_N is reduced by a factor of 2 for CeRhIn_5 ($T_N \sim 4$ K) compared to CeIn_3 ($T_N \sim 10$ K), which is just the opposite of the situation in NdRhIn_5 and NdIn_3 .

These contrary behaviors may be understood by noticing that the magnetic moments in CeRhIn_5 lie in the ab plane,¹⁹ whereas the CEF anisotropy tends to favor energetically the Ce spins to point along the c axis.^{2,21} Therefore there might be in CeRhIn_5 competing anisotropic magnetic interactions that lead to an incommensurate magnetic state at lower T_N when compared to CeIn_3 . Accordingly, field-dependent heat capacity²² has revealed a rich H - T phase diagram with field-induced transitions similar to what was observed in NdIn_3 , where competing CEF and exchange interaction anisotropies were considered.

Alternatively, antiferromagnetic correlations across the intervening RhIn_2 layers in NdRhIn_5 are in some sense more reminiscent of Ce_2RhIn_8 , in which the magnetic structure within CeIn_3 bilayers are unmodified relative to cubic CeIn_3 and the correlations across the RhIn_2 layers are antiferromagnetic.²³

In conclusion, we find a commensurate antiferromagnetic structure, as represented in Fig. 3, with $\mathbf{q}_M=(\frac{1}{2}0\frac{1}{2})$ for NdRhIn_5 . The staggered Nd moment is determined at 1.6 K to be $2.5(1)\mu_B$ aligned along the tetragonal c axis. The phases of the nearest-neighbor Nd atoms are the same as in the commensurate phase of cubic NdIn_3 .

Work at Los Alamos was performed under the auspices of the U.S. Department of Energy. H.N. acknowledges support from the NSF (grant number DMR-0094241).

*Electronic address: schang@nmsu.edu

¹Y. N. Grin, Y. P. Yarmolyuk, and E. I. Giadyshevskii, *Sov. Phys. Crystallogr.* **24**, 137 (1979).

²H. Hegger, C. Petrovic, E. G. Moshopoulou, M. F. Hundley, J. L. Sarrao, Z. Fisk, and J. D. Thompson, *Phys. Rev. Lett.* **84**, 4986 (2000).

³C. Petrovic, P. G. Pagliuso, M. F. Hundley, R. Movshovich, J. L. Sarrao, J. D. Thompson, Z. Fisk, and P. Monthoux, *J. Phys.: Condens. Matter* **13**, L337 (2001).

⁴C. Petrovic, R. Movshovich, M. Jaime, P. G. Pagliuso, M. F. Hundley, J. L. Sarrao, Z. Fisk, and J. D. Thompson, *Europhys. Lett.* **53**, 254 (2001).

⁵S. Kawasaki, T. Mito, G. Q. Zheng, C. Thessieu, Y. Kawasaki, K. Ishida, Y. Kitaoka, T. Muramatsu, T. C. Kobayashi, and D. Aoki, *Phys. Rev. B* **65**, 020504 (2001).

⁶R. Movshovich, M. Jaime, J. D. Thompson, C. Petrovic, Z. Fisk,

P. G. Pagliuso, and J. L. Sarrao, *Phys. Rev. Lett.* **86**, 5152 (2001).

⁷K. Izawa, H. Yamaguchi, Y. Matsuda, H. Shishido, R. Settai, and Y. Onuki, *Phys. Rev. B* **63**, 057002 (2001).

⁸S. Doniach, in *Valence Instabilities and Related Narrow Band Phenomena*, edited by R. D. Parks (Plenum, New York, 1977).

⁹J. Jensen and A. R. Mackintosh, *Rare Earth Magnetism: Structures and Excitations* (Oxford University Press, Oxford, 1991).

¹⁰P. G. Pagliuso, J. D. Thompson, M. F. Hundley, and J. L. Sarrao, *Phys. Rev. B* **62**, 12 266 (2000).

¹¹G. L. Squires, *Introduction to the Theory of Thermal Neutron Scattering* (Cambridge University Press, Cambridge, 1978).

¹²M. Blume, A. J. Freeman, and R. E. Watson, *J. Chem. Phys.* **37**, 1245 (1962).

¹³K. H. J. Buschow, H. W. D. Wijn, and A. M. V. Diepen, *J. Chem. Phys.* **50**, 137 (1969).

- ¹⁴A. Czopnik, N. Iliw, B. Stalinski, C. Bazan, H. Madge, and R. Pott, *Physica B* **130**, 259 (1985).
- ¹⁵A. Czopnik, J. Kowalewski, and M. Hackemer, *Phys. Status Solidi A* **127**, 243 (1991).
- ¹⁶S. Mitsuda, P. M. Gehring, G. Shirane, H. Yoshizawa, and Y. Onuki, *J. Phys. Soc. Jpn.* **61**, 1469 (1992).
- ¹⁷M. Amara, R. M. Galéra, P. Morin, T. Veres, and P. Burlet, *J. Magn. Magn. Mater.* **130**, 127 (1994); M. Amara, R. M. Galéra, P. Morin, J. Voiron, and P. Burlet, *ibid.* **131**, 402 (1994); **140-144**, 1157 (1994).
- ¹⁸P. G. Pagliuso *et al.* (private communication).
- ¹⁹W. Bao, P. G. Pagliuso, J. L. Sarrao, J. D. Thompson, Z. Fisk, J. W. Lynn, and R. W. Erwin, *Phys. Rev. B* **62**, R14 621 (2000); **63**, 219901(E) (2001).
- ²⁰N. J. Curro, P. C. Hammel, P. G. Pagliuso, J. L. Sarrao, J. D. Thompson, and Z. Fisk, *Phys. Rev. B* **62**, R6100 (2000).
- ²¹P. G. Pagliuso, N. J. Curro, N. O. Moreno, M. F. Hundley, J. D. Thompson, J. L. Sarrao, and Z. Fisk, *Physica B* **320**, 370 (2002).
- ²²A. L. Cornelius, P. G. Pagliuso, M. F. Hundley, and J. L. Sarrao, *Phys. Rev. B* **64**, 144411 (2001).
- ²³W. Bao, P. G. Pagliuso, J. L. Sarrao, J. D. Thompson, Z. Fisk, and J. W. Lynn, *Phys. Rev. B* **64**, 020401 (2001).